ELSEVIER

Catena 46 (2001) 141–157

CATENA

www.elsevier.com/locate/catena

# Microrelief induced by tillage: measurement and modelling of Surface Storage Capacity

Olivier Planchon [a,*], Michel Esteves [b], Norbert Silvera [a], Jean-Marc Lapetite [b]

[a] *Institut de Recherche pour le Développement (IRD), BP 1386, Dakar, Senegal*
[b] *Laboratoire d'étude des Transferts en Hydrologie et Environnement (LTHE), BP 53, 38041 Grenoble Cedex 9, France*

**Abstract**

The micro-topography of a groundnut plot in Senegal has been recorded over a full cultivation cycle, using an automated device able to measure 16.2 $m^2$ at every 5 cm with an accuracy of 1 mm. Tillage is horse drawn, perpendicular to the general slope, and generates oriented microreliefs. Surface Storage Capacity (SSC) was calculated on both raw and slope-detrended surfaces. Additionally, various boundary conditions (BC) were used: no-wall; three-wall (up, left and right); or mirror (the Digital Elevation Model (DEM) surrounded by eight alternately reversed images of itself). SSC is more affected by these variants than by the variations of microrelief itself. Whatever the calculation method, SSC (as well as random roughness), follows a decreasing exponential with cumulated rainfall, but the coefficients of the exponential differ widely to each other. This suggests that SSC values could be of little use when they are obtained on various slopes, arbitrarily detrended or not, and calculated with arbitrary BC. We suggest a simple geometric model to characterise the way microrelief empties as the slope increases. The model has two calibrated depth-ratio parameters, one in each direction. It gives a more coherent framework for calculation and use of SSC. The model was applied to one of the DEMs of the data set, sampled after the first rain following hoeing. With the mirror-BC and detrended slope, SSC was 3.6 mm. Microrelief was found to behave in the same proportions, when tilted, than a tetrahedral container 94 times wider than deeper in the tillage direction and 11 times perpendicularly. This model represents the volume of surface water that cannot flow in any direction. With three-wall-BC, SSC was 6.7 mm, 1.4 mm remaining on the plot whatever the slope angle, and 5.3 mm behaving the same as a container 69 times wider than deeper. A possible use of this model is illustrated with

* Corresponding author. Fax: +221-820-43-07.
*E-mail address:* Olivier.Planchon@IRD.sn (O. Planchon).

0341-8162/01/$ - see front matter 
PII: S0341-8162(01)00163-1

an attempt to upscale the sampled plot to the watershed to which it belongs. 

*Keywords:* Microrelief; Soil roughness; Surface Storage Capacity; DEM; Senegal

## 1. Introduction

Most erosion models show a poor accuracy at rainfall-catchment scale. A number of mismatches between measured and modeled soil losses are reported by Nearing (1998) and Mitas and Mitasova (1998). According to the analysis of Jetten et al. (1999), an important reason of these problems is the poor knowledge of soil surface properties. This situation certainly originates from a lack of widespread and standardized microrelief data. However, the situation changes quickly. Relief-meters providing Digital Elevation Models (DEMs) on one or several square meters with millimetric to centimetric space resolutions becomes more and more available (Römkens et al., 1986; Huang and Bradford, 1990a; Helming et al., 1993; Wilson et al., 1994; Magunda et al., 1997; Kamphorst, 2000; Planchon et al., 2000a,b among others) and many studies have focused their interest in the analyses of these data.

Surface Storage Capacity (SSC) is one of these crucial parameters for runoff-erosion models. It is most often calculated numerically when microrelief data is available (Planchon and Darboux, 2001, gave a fast algorithm for that). Few studies measured SSC physically, by filling with water a sample of the soil surface after coating it with impervious material (Gayle and Skaggs, 1978), or making a replica in resin (Kamphorst, 2000). When microrelief is unknown, SSC can be deduced from random roughness. Huang and Bradford (1990b) analysed this relation from a theoretical point of view. Mwendera and Feyen (1992) proposed a formula from their own experimental data and Kamphorst et al. (2000) found SSC = 0.28 RR, with $r^2 = 0.8$ on a large collection of microrelief data.

Most papers dealing with SSC focused their interest on the sampled area. They consider its properties for itself rather than as a part of the whole field. Kamphorst (2000), for example, used a laser relief-meter to measure the SSC of resin-moulded surfaces duplicated from agricultural fields. Then, she verified the measurements by weighting the water contained in the mouldings. However, the success of this verification could not get her further away from the main question, which still remains an open issue: can we estimate the SSC of a field from a sample of its microrelief? This problem is so rarely tackled that confusion still remains on the definition of SSC.

Looking at a whole cultivated field, SSC is widely recognized as the mean depth of the largest volume of water the studied area can store at the soil surface before runoff occurs at its boundary. A certain confusion remains, however, on the precise definition of SSC of an area of a few square meters sampled in this field. In this study, we refer to the SSC of a sample as the largest volume of water it can store in its native location in the field. Any attempt to negate the natural environment of the sampled microrelief could only lead to estimations of SSC, which are denoted $\overline{SSC}$ in this paper. Stated that

way, estimating SSC is the final objective. Calculating $\overline{SSC}$ on a given sample is an intermediate objective, and all methods used to obtain $\overline{SSC}$ should be justified in this context.

Two major issues are then raised: the boundary condition (BC) applied to the sample, and the way to consider the slope of the sampled terrain.

- *Influence of boundary condition*: Everybody has observed a ploughed field after rainfall: narrow puddles stretch for tens of meters between ridges. Estimating their volume from a sampled microrelief of only a few square meters crucially raises the issue of the choice of an adequate BC. More often, the sample is bordered with three walls, leaving open the side oriented downwards in the original location of the sample. This BC is almost a standard and will be denoted as the three-wall-BC. Other BCs can be used. The no-wall-BC allows free drainage through all directions. Planchon et al. (1998), followed by Kamphorst et al. (2000) proposed the mirror-BC, which consists in surrounding the sample with eight mutually inverted images of itself (Fig. 1). In any case, choosing a BC is an inevitable prerequisite for calculating $\overline{SSC}$.
- *Influence of slope*: Slope is recognized as an important factor governing $\overline{SSC}$ (Onstad 1984; Mwendera and Feyen, 1992, Kamphorst et al., 2000). In the close proximity of horizontality, $\overline{SSC}$ decreases quickly when the sample is tilted (Mwendera and Feyen, 1992). Therefore, this poses the problem of choosing an appropriate slope treatment. Calculating $\overline{SSC}$ on raw data ties the result to the precise location of the sample. On the other hand, subtracting the slope before calculating $\overline{SSC}$ leads to an overestimated result, which is useless until the relation between slope and $\overline{SSC}$ is known. Additionally, the influence of slope depends on its direction compared with the tillage direction.

In this paper, we used a series of microrelief measurements made in a plot of $4 \times 4$ m during a full cultivation cycle. The data set is used to show the importance of the choice of the BC and the slope detrending. Therefore, we propose a simple geometric model, which allows the issues of BC and slope detrending to be integrated into a single conceptual frame. A possible use of this model is illustrated by an attempt to upscale the sampled plot to the watershed to which it belongs.

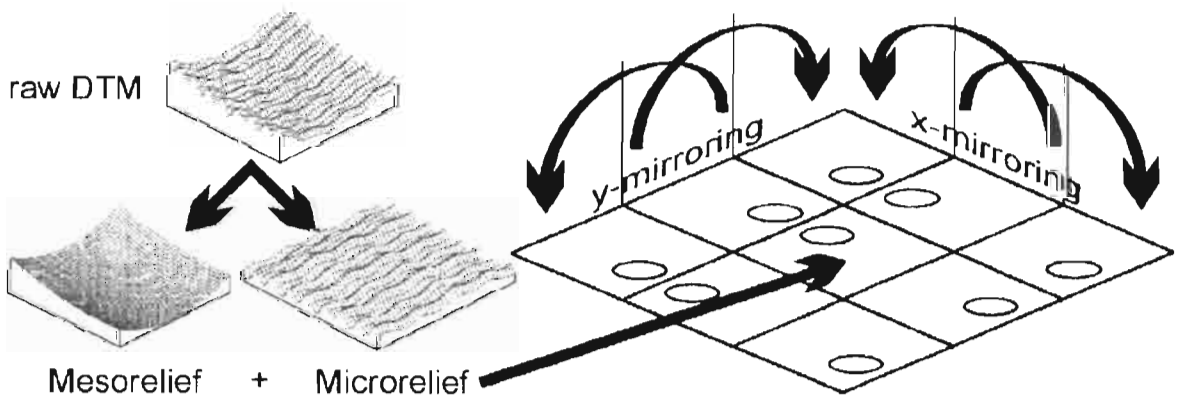


Fig. 1. Diagram of the mirror-BC method.

## 2. Material and methods

### 2.1. The study area

The experiment took place in a 2.85-ha catchment of Thysse Kaymor, a village in the Senegalese groundnut belt. The slope gradient is under 1.5% in 95% of the area. The median slope gradient is 0.73%. The area is cultivated with millet-groundnut rotation (Perez, 1994). Tillage is horse-drawn, perpendicular to the slope. Three erosion plots, 50 $m^2$ each, had been set up in this catchment. They were bordered with metal sheets that were removed to allow the farmer to till the plots and the surrounding fields the same way. Microrelief was sampled in a 16.2-$m^2$ area at the center of each erosion plot. The data used for this study came from the groundnut plot, in which tillage was spaced at every 50 cm. From June 28th to October 13th 1997, 19 Digital Elevation Models (DEMs) with a 5-cm cell size were collected, and 3 with a 2.5-cm cell size. This corresponds to one measurement after almost each soil surface change (rainfall or tillage).

### 2.2. The electronic relief meter

Microrelief was measured with an electronic relief meter (Fig. 2) designed and constructed at the IRD research center in Dakar, Senegal. This device includes a transportable frame, which is 4.5 m wide and 1.2 m high. A transversal beam moves on the frame. A carriage moves on the beam and guides a vertical rod with a sensor at the end. When the sensor contacts the soil surface, the $X$, $Y$ and $Z$ co-ordinates of the sensor are recorded in the control panel's static memory. The measurement of each point requires 0.6 s. After the end of each measurement, the control panel is unplugged from the relief meter and connected to the serial port of a computer to download the data.

The frame was tied to four bases set up on the plot and anchored at a depth of 50 cm in the soil. During the experiment, a certain number of rows were measured twice to determine the accuracy of the measurement. The standard deviations evaluated by this way were, respectively, 0.85 mm in the $Z$ direction (elevation error), and 6 mm in the $X$ and $Y$ directions (position error). The position error was mainly due to wind, which caused oscillations of the beam and the rod. These problems have been fixed in the latest version of the device.

### 2.3. Random roughness (RR)

Allmaras et al. (1966) defined Random Roughness as the standard deviation of elevations after the slope and tillage effects were removed and the upper and lower 10% of the measurements were eliminated. They used a logarithm transformation of the raw data but the pertinence of this transformation was contested later (Currence and Lovely, 1970). Furthermore, as reported by Zobeck and Onstad (1987), it is sometimes difficult to determine whether or not all details of the Allmaras et al. (1966) procedure were carried out in a given study. Moreover, Allmaras et al. (1966) did not give any indication on the procedure used to remove tillage effects. We propose here a formula for simultaneously removing slope and tillage effects and calculating the standard

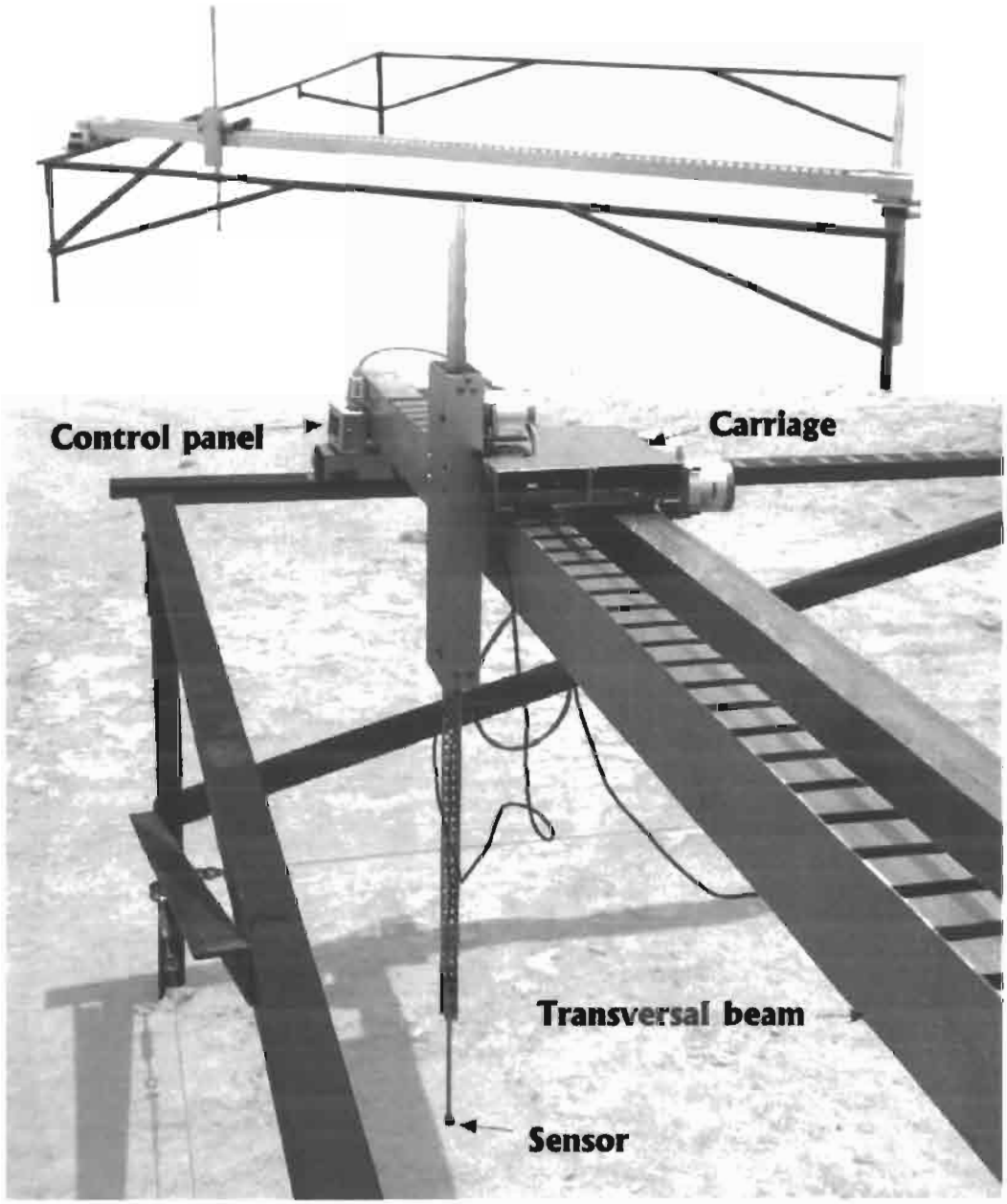


Fig. 2. The electronic relief-meter.

deviation of the residuals (Eq. (1)). It consists of subtracting to each point the mean of its own row and the mean of its own column (Eq. (1)). This procedure gives each row and each column a zero-average. Therefore, slope effects are removed in all cases, and tillage effects are removed when tillage follows one of the directions of the lattice, which is the case in most datasets.

$$\mathrm{RR} = \sqrt{\frac{\sum_{i,j}\left(z_{i,j} - z_{i,\cdot} - z_{\cdot,j} + z_{\cdot,\cdot}\right)^2}{n-1}} \tag{1}$$

where $i$ and $j$ are rows and columns indexes; $z_{i,\cdot}$, $z_{\cdot,j}$, $z_{\cdot,\cdot}$ are the mean value of row $i$, column $j$, and all the data, respectively; and $n$ is the number of cells.

### 2.4. Surface Storage Capacity (SSC)

We used the algorithm described by Planchon and Darboux (2001) for calculating SSC. Each cell represents a small square horizontal area and eight neighbours are considered. These two points have been widely adopted after the work of Moore and Larson (1979). Contrary to the algorithms of Moore and Larson (1979) and Jenson and Domingue (1988), which gradually fill depressions and merge the embedded ones, this algorithm first adds a thick layer of water on the whole area and then iteratively removes the water in excess. Results are identical to Jenson and Domingue (1988) but it is simpler and dramatically faster. Note that all algorithms, including Planchon and Darboux (2001), use a no-wall-BC. Surrounding the DEM with dummy cells of appropriate elevation simulates other BCs.

### 2.5. Slope detrending and boundary conditions (BCs)

As mentioned in the Introduction, $\overline{\mathrm{SSC}}$ closely depends on the BC used and the slope treatment, i.e. using raw or slope-detrended surfaces. These points are noted in this paper by the mean of a subscript for slope treatment, and a superscript for BC. Table 1 shows these notations.

Detrended surfaces were obtained with a quadratic least-square adjustment rather than a planar adjustment because the sampled area was slightly concave (11 mm at the center), which was considered as a side effect cause by its particular location at the center of an erosion plot. The following equation gives the elevation $z$ of the adjusted quadratic shape, where $x$ and $y$ are the co-ordinates across, and along the main slope, respectively. All values are in meters.

$$z(x,y) = \left(5.7807y + 0.77202y^2 + -7.433x + 2.7171x^2 + -0.20315xy - 14.37\right) \times 10^{-3}.$$

The combination of the two slope treatment (raw or detrended) and three BCs (no-wall, three-wall and mirror) led to four methods for calculating $\overline{\mathrm{SSC}}$ (Table 1). $\overline{\mathrm{SSC}}^{R}_{3\mathrm{W}}$ is the most common estimation of SSC; almost a standard. Fig. 1 illustrates the mirror-BC, which is fairly new. Applying this BC to a sloping DEM could generate

Table 1
Notations of the various combinations of slope treatment and BCs

| | Mirror-BC | Three-wall-BC | No-wall-BC |
|---|---|---|---|
| Raw data | (not pertinent) | $\overline{\mathrm{SSC}}^{R}_{3\mathrm{W}}$ | $\overline{\mathrm{SSC}}^{R}_{\mathrm{NW}}$ |
| Slope-detrended | $\overline{\mathrm{SSC}}^{0}_{\mathrm{M}}$ | $\overline{\mathrm{SSC}}^{0}_{3\mathrm{W}}$ | (not used) |
| Slope-detrended, then tilted | $\overline{\mathrm{SSC}}^{a,b}_{\mathrm{M}}$ | $\overline{\mathrm{SSC}}^{a}_{3\mathrm{W}}$ | (not used) |

$b$ and $a$ are the angles of tilt in the tillage direction and perpendicularly to it, respectively.

Table 2
$\overline{SSC}^{R}_{NW}$ (mm) calculated on the re-sampled DEMs (5-cm cells) compared to the originals (2.5-cm cells)

| Date | 2.5 cm DEM | 5 cm re-sampled DEMs | | | | Mean and 95% C.I. |
|---|---|---|---|---|---|---|
| Sept 6th | 3.88 | 4.00 | 3.97 | 3.84 | 3.94 | 3.94 mm ± 0.13 |
| Sept 11th | 2.26 | 2.16 | 2.38 | 2.32 | 2.11 | 2.24 mm ± 0.25 |
| Oct 12th | 1.78 | 1.77 | 1.78 | 1.76 | 1.75 | 1.77 mm ± 0.03 |

facets. Therefore, it is only used on slope-detrended DEMs. The water stored in these conditions represents, in the field, the volume of water which cannot flow in any direction. $\overline{SSC}^{0}_{3W}$ represents, in the field, the volume of water which cannot run in the direction of the terrain slope but, when tillage is almost perpendicular to the slope direction, can run along those furrows which are slightly sloping (that will happens when the 'walls' are removed).

These values could be of interest in hydrological models while they represent important thresholds governing the early stages of runoff.

### 2.6. Accuracy of the space resolution of the DEMs

Three DEMs with a 2.5-cm cell size were used to verify whether the 5-cm space resolution, used in the rest of the data set, is appropriate. To do that, these DEMs were re-sampled so that each of them gave four different DEMs at 5 cm, starting the re-sampling with the first and the second cell of the first and the second row, respectively. $\overline{SSC}^{R}_{3W}$ was calculated on the re-sampled DEMs and compared to the value of the original DEM. The results (Table 2) show that the 5-cm space resolution is precise enough ($\pm 0.25$ mm in the worst case) and unbiased (all values at 2.5 cm are in the confidence interval of the re-sampled DEMs). We conclude that the 5-cm space resolution was appropriate to the studied microreliefs.

## 3. Tetrahedral model of SSC

The sum of all the puddles acts the same way as a single container emptying while tilted. A container with a right angle triangular section is used to model this behaviour. The section's area is $V = HL/2$ (Fig. 3). When it is tilted at angle $\alpha$, the remaining volume is $V' = H'L'/2$. The percentage of water remaining $V'/V$ is calculated in the following equations (notations are explained in Fig. 3):

$$V'/V = (H'/H)(L'/L). \tag{2}$$

Let: $a = \tan(\alpha)$: tilt gradient of container, $k = 1/\tan(\gamma)$ (i.e. $k = L/H$): depth coefficient of container.

Let us consider that:

$$H'/H = \cos(\alpha) \tag{3}$$

$$L' = h/\sin(\alpha) \tag{4}$$

$$h = L\tan(\alpha)\tan(\gamma)/(\tan(\alpha) + \tan(\gamma)). \tag{5}$$

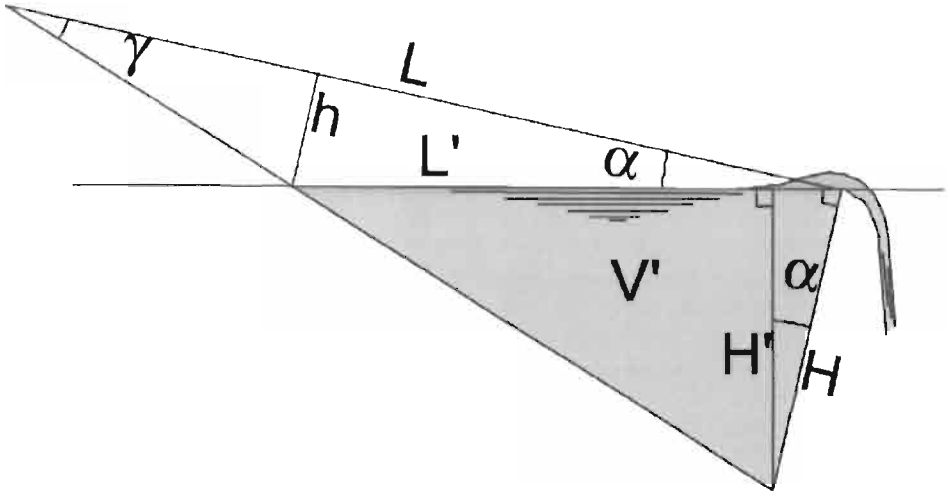


Fig. 3. Cross-section diagram of a container with triangular section, which empties at the same rate as the plot according to the angle of tilt $\alpha$. Notations are those of Eqs. (3)–(8).

Then substituting Eqs. (3)–(5), in Eq. (2) and simplifying yields:

$$V'/V = 1/(1 + ak). \tag{6}$$

For the same angle of tilt, the remaining volume is a function of the depth coefficient $k$. When $k$ is small, the container is deeper than wider and can contain water even when tilted. When $k$ is large, we have a shallower container that empties easily.

In three dimensions, the container used as a model is a reverse tetrahedron with three right angles at the apex O (Fig. 4). Each perpendicular cross-section corresponds to the triangle of Fig. 3. We used the same notations as in Fig. 3 with the subscripts 'l' and 't' in the longitudinal and perpendicular directions of the furrows, respectively.

The volume of a tetrahedron is equal to one-third of its base by its height. The base of the initial tetrahedron is $L_l L_t/2$ and its height is $H$. When tilted, the base becomes

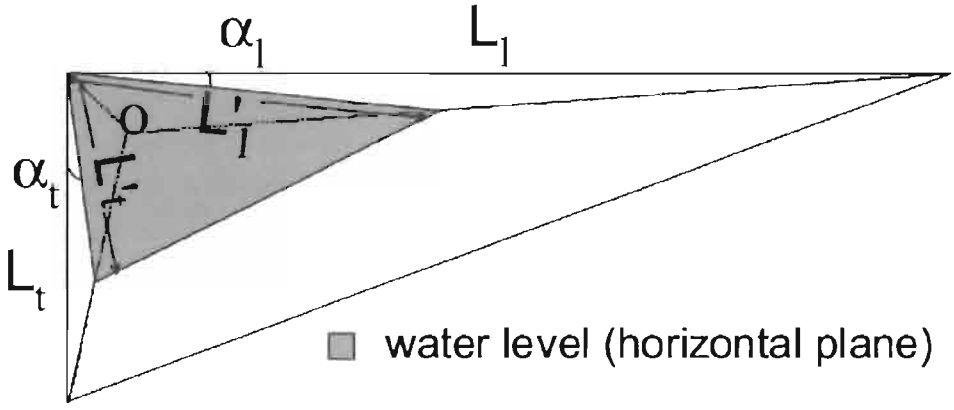


Fig. 4. Diagram of a tetrahedral container (seen from above), which empties at the same rate as the plot according to the longitudinal $\alpha_l$ and transversal $\alpha_t$ angles of tilt. The notations are those of Eqs. (7) and (8).

$L'_l L'_t/2$ and the height, $H \cos(\alpha_l) \cos(\alpha_t)$ (Fig. 4). After simplifications, the ratio $V'/V$ is given by the following equation:

$$V'/V = (\cos(\alpha_l) L'_l/L_l)(\cos(\alpha_t) L'_t/L_t). \quad (7)$$

Eq. (3) can be substituted in each of the two members of the product at the right of Eq. (7). Then, replacing Eq. (3) by its result, given in Eq. (6), yields the final equation:

$$V'/V = 1/((1 + a_l k_l)(1 + a_t k_t)). \quad (8)$$

This model allows us to calibrate separately the depth coefficients $k_l$ and $k_t$ by tilting the DEM in the corresponding directions. Therefore, it is not necessary to tilt the DEM in all directions but only in two orthogonal ones. We have calibrated the model this way. The values of SSC calculated in the other directions were used for validation.

## 4. Results

### 4.1. Time variability and effects of BCs and slope-detrending

Fig. 5 shows the evolution of the soil surface parameters during the crop cycle. Vertical solid lines show the rainfall events and their depths (in millimeters on the

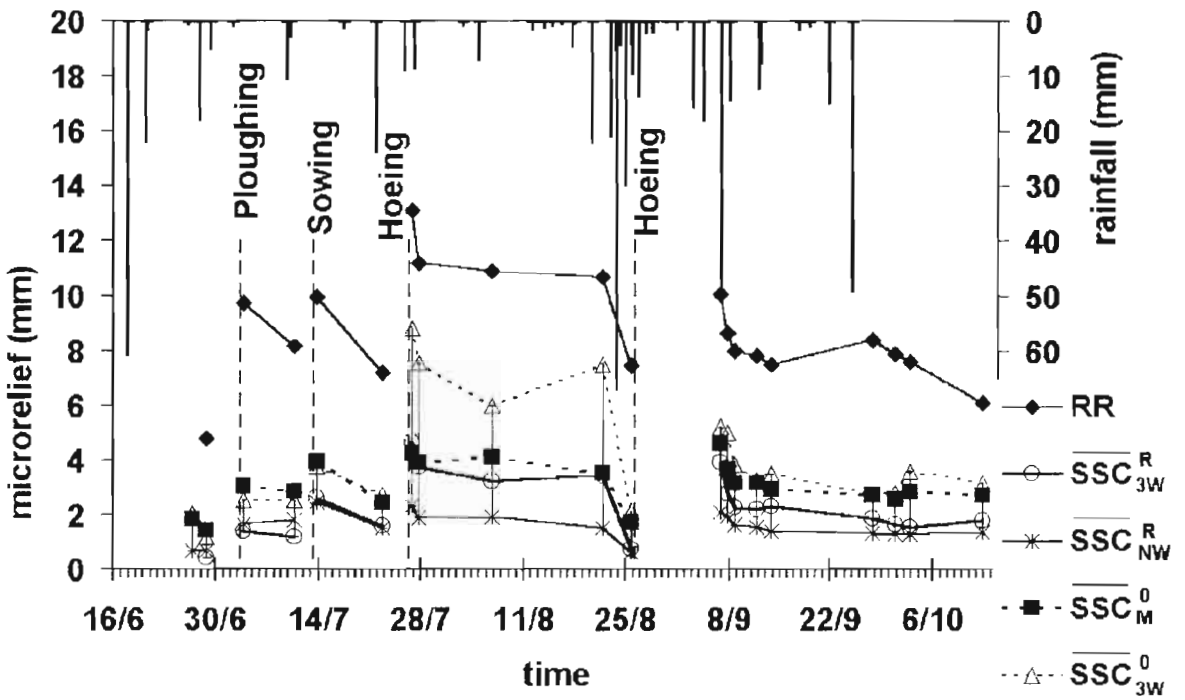


Fig. 5. $\overline{SSC}$ calculated after various data treatment (see Table 1), and Random Roughness (RR), during the vegetation cycle.

right-hand scale). Lines representing $\overline{SSC}^{R}_{3W}$ and RR (in millimeters on the left-hand scale) are discontinued at each working of the soil. Fig. 5 shows that RR and $\overline{SSC}$ increase at the working of the soil, particularly at hoeing, and decrease after the following rains. It also shows that the variability of $\overline{SSC}$ values at a given time, as caused by the use of various calculation methods (including BC and slope detrending), is greater than the variability along the whole cycle for a given calculation method.

At a given timing, the values are almost always in the same decreasing order. The highest values are calculated from slope-detrended surfaces ($\overline{SSC}^{0}_{3W}$, followed by $\overline{SSC}^{0}_{NW}$), Values calculated from raw surfaces are below, and close to each other. This shows how slope can be an important factor in SSC. $\overline{SSC}^{0}_{3W}$ significantly differs from others just after hoeing (July 26th) and remains different until a heavy storm caused runoff and consequently opens the ridges (August 26th). After the second hoeing, no data were taken before the big storm of September 7th (50 mm) and all $\overline{SSC}$ values are low and close to each other.

Fig. 6 shows the variation of $\overline{SSC}$ and RR with the cumulated rainfall since hoeing. Both $\overline{SSC}$ and RR adjust to decreasing exponential in the form of Eq. (9). Table 3 shows the three calibrated parameters of Eq. (9).

$$y = M(1 - K(1 - \exp(-h\ln(2)/H)) \tag{9}$$

where $h$ (in mm) is the cumulated rainfall depth since hoeing; $M$ (in mm) is the initial value of $y$; $K$ $(0 < K < 1)$ is the maximum proportion of $M$ which can be lost; $H$ (in mm) is the half-life parameter of the exponential.

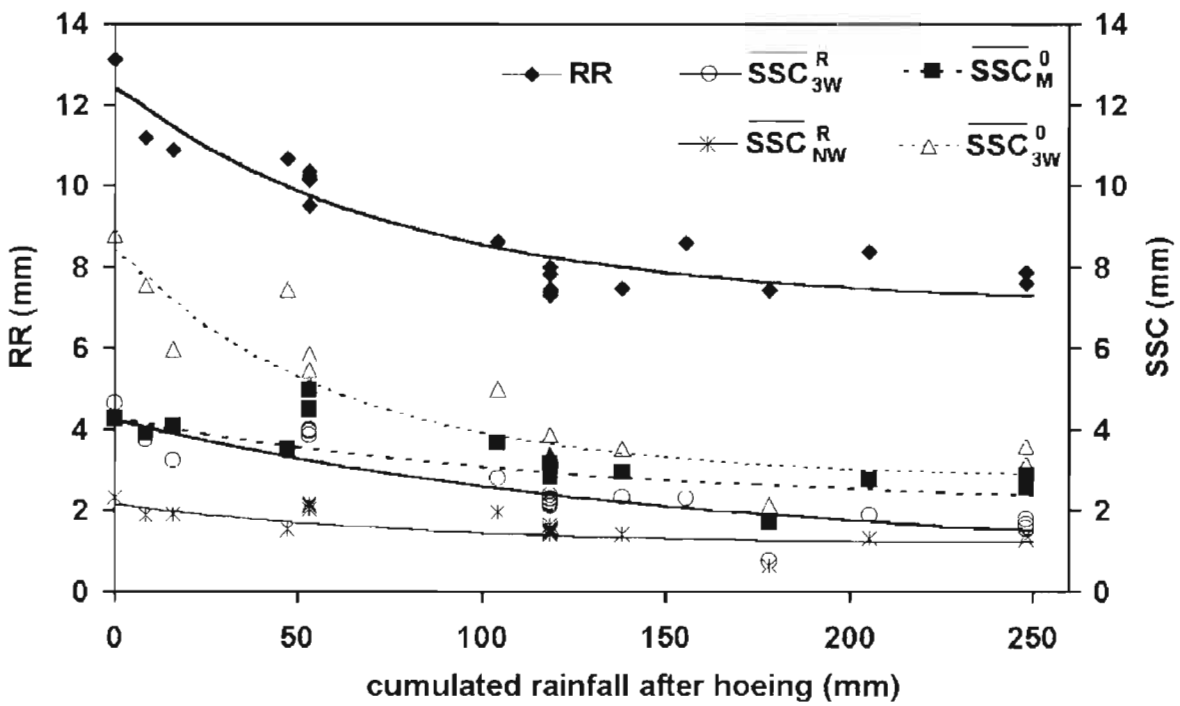


Fig. 6. $\overline{SSC}$ calculated after various data treatment (see Table 1), and Random Roughness (RR), related to the depth of cumulated rainfall after hoeing.

Table 3
Parameters of the exponential decrease of RR and SSC with cumulated rainfall depth after hoeing (Eq. (9))

| | $M$ (mm) | $K$ (ratio) | $H$ (mm) |
|---|---|---|---|
| $\overline{SSC}^{R}_{3W}$ | 4.23 | 0.79 | 104.7 |
| $\overline{SSC}^{0}_{3W}$ | 8.45 | 0.67 | 43.2 |
| $\overline{SSC}^{R}_{NW}$ | 2.15 | 0.46 | 56.0 |
| $\overline{SSC}^{0}_{M}$ | 4.31 | 0.51 | 86.1 |
| RR | 12.44 | 0.43 | 53.3 |

The no-wall BC and the three-wall-BC gave the lowest values of $K$ (Fig. 6 and Table 3), which means that these BCs describe a storage capacity less affected by cumulated rainfalls: they represent small discontinuous puddles at the bottom of the furrows. On the other hand, the three-wall-BC gave the highest values of $K$, therefore describing a storage capacity more affected by cumulated rainfalls. This is because after tillage, the ridges are high and intact, but this situation does not remain stable. When they are cut by runoff, $\overline{SSC}^{0}_{3W}$ converges towards $\overline{SSC}^{0}_{M}$.

Fig. 7 illustrates the relations between $\overline{SSC}$ and RR. They are close and linear, which is in agreement with previous studies, both from experimental data (Onstad, 1984) and

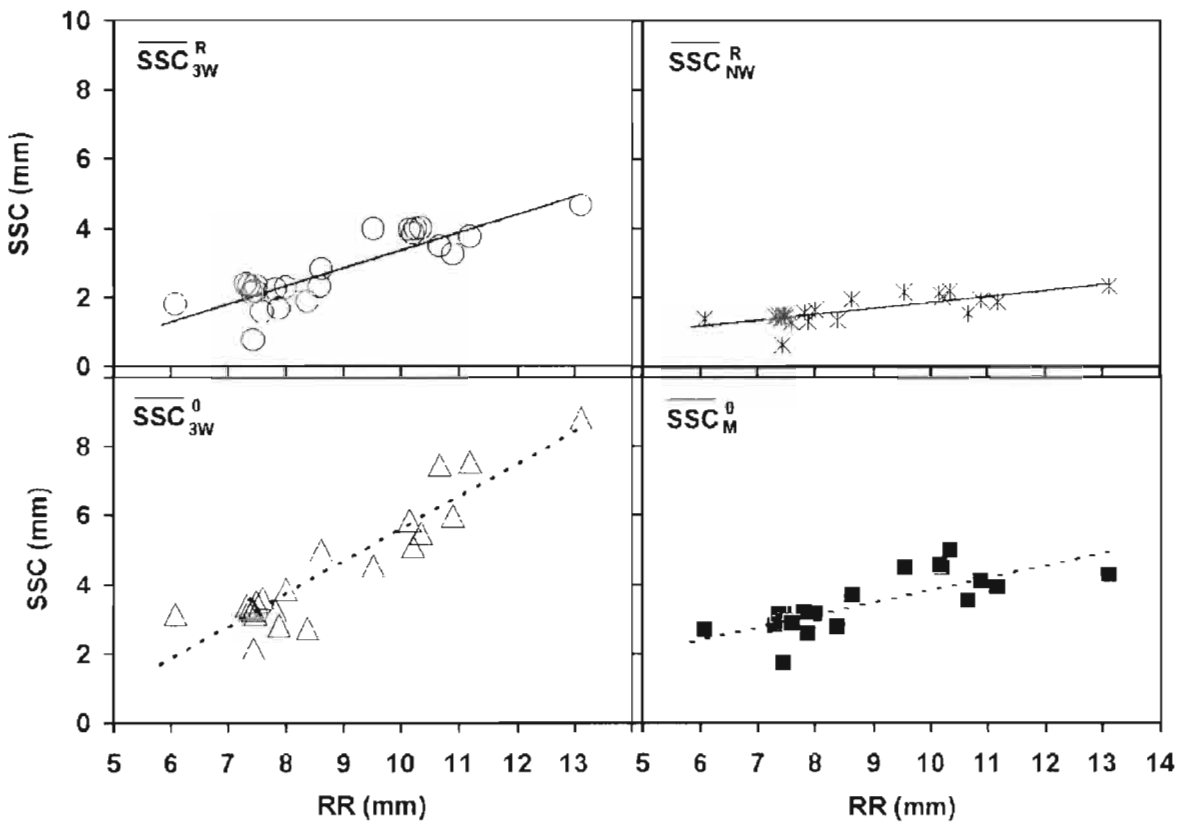


Fig. 7. $\overline{SSC}$ calculated after various data treatment (see Table 1) related to Random Roughness (RR).

from a theoretical point of view (Huang and Bradford, 1990b), but however, each of the four regression lines shown by Fig. 7 is very different. This sensitivity to the BC used, and to the choice between raw or detrended slope, lessens the usefulness of equations relating SSC to RR in the case of tillage-induced microreliefs.

In conclusion, this first part of the results shows that slope and BCs are determining factors in the evaluation of SSC. Results vary more with the calculation method than with time, over the crop cycle, for each method. This raises dramatically the question of the significance and the usefulness of $\overline{SSC}$, when estimated from a small microrelief sample.

In the second part of this study, the tetrahedral model described above is validated. Then, the physical significance of different BCs is discussed.

### 4.2. Validation of the tetrahedral model

In this section, we used the DEM of July 27th. The plot was tilled on the 26th and 10 mm of rain fell that night. This small rainfall created a situation that was more representative of hydraulic properties of microrelief than the situation of the day before, just after tillage (Planchon et al., 2000a show that microrelief of these sandy soils changes very quickly during the first millimeters of rain after tillage).$\overline{SSC}_M^{a,0}$, $\overline{SSC}_M^{0,b}$, and $\overline{SSC}_{3W}^{a}$ (see Table 1 for notations) were calculated for angles of tilt from 0% to 5% by increments of 0.1% (Fig. 8). Eq. (6) has a single coefficient to calibrate: $k$. $\overline{SSC}_M^{a,0}$ and $\overline{SSC}_M^{0,b}$ are in excellent agreement with this equation, with values of $k$ of 11 and 94, respectively, and coefficients of determination over 99%. $\overline{SSC}_{3W}^{a}$, however, required an

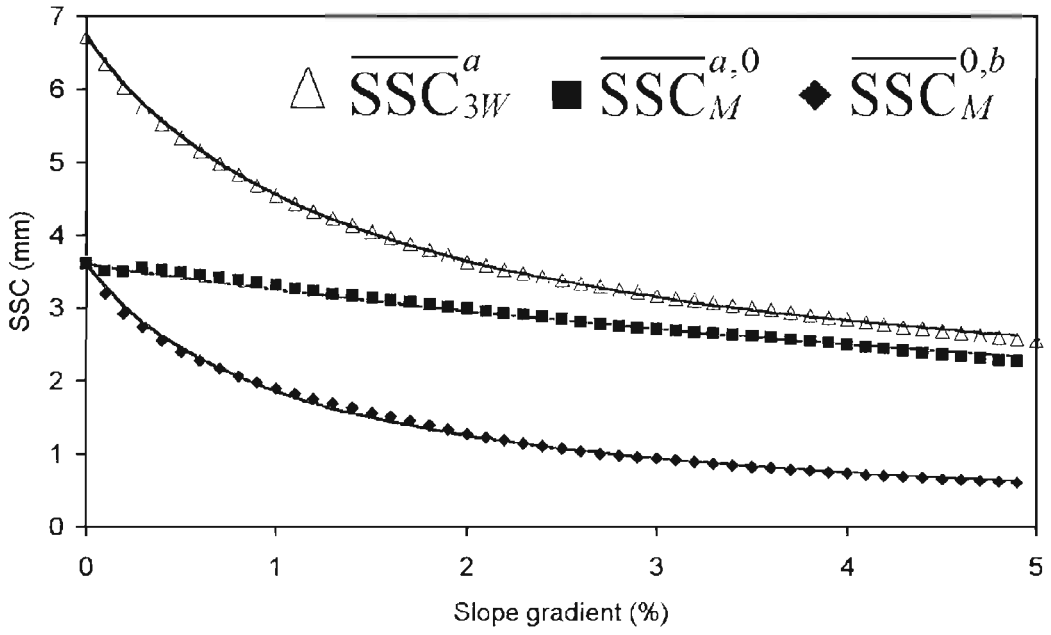


Fig. 8. Decrease of $\overline{SSC}$ with increasing slope gradient. Values calculated (dots) on the DTM of July 27th and modelled (lines) according to Eq. (6) ($\overline{SSC}_M^{a,0}$ and $\overline{SSC}_M^{0,b}$) or to Eq. (10) ($\overline{SSC}_{3W}^{a}$).

additional calibrated coefficient to represent a part of SSC which could not flow across the furrows Eq. (6) was therefore modified in Eq. (10):

$$\overline{SSC}^{a}_{3W} = SSC_{min} + (SSC_{max} - SSC_{min})/(1 + ka). \quad (10)$$

The measured value of $SSC_{max}$ was 6.71 mm. The adjustment yield $SSC_{min} = 1.41$ mm; $k = 69$; $r^2 = 99.93\%$.

This first part of the results shows excellent agreement of the tetrahedral model used in one dimension, as long as an additional coefficient, $SSC_{min}$, can be introduced when required. The next step of the validation is to compare the model to the measured $\overline{SSC}$ after the surface was tilted in all directions.

Fig. 9a shows the values of $\overline{SSC}^{a,b}_{M}$ calculated by tilting the DEM from 0% to 5% by increments of 0.1% and in all the directions from 0° to 180° by increments of 10°, making 950 calculations of SSC on 238 by 241 DEMs, which was made possible thanks to the fast algorithm given by Planchon and Darboux (2001).

Fig. 9b shows the result of the tetrahedral modelling according to Eq. (8) with the depth ratios of 11 and 94. The two figures are close to each other. Correlation coefficient $r^2$ is 91.3%. The residuals mean is 0.11 mm and their standard deviation is 0.07 mm. The bias of 0.11 mm can reach 0.25 mm in the direction 45° for the lowest values of SSC. The explanation of the bias is that the equation of the true decrease of SSC in one direction is not fully independent of the angle of tilt in the perpendicular direction, as the model supposes it to be. Fig. 9a shows indeed that, over 3% of slope along the furrows, SSC becomes less dependent of the perpendicular slope gradient.

In conclusion, the model of Eq. (9) is acceptable, with a small bias. The three parameters of the model have a straightforward geometric meaning: the measured maximum capacity of the container and its calibrated depth ratios $k_l$ and $k_t$ in the two orthogonal directions, respectively.

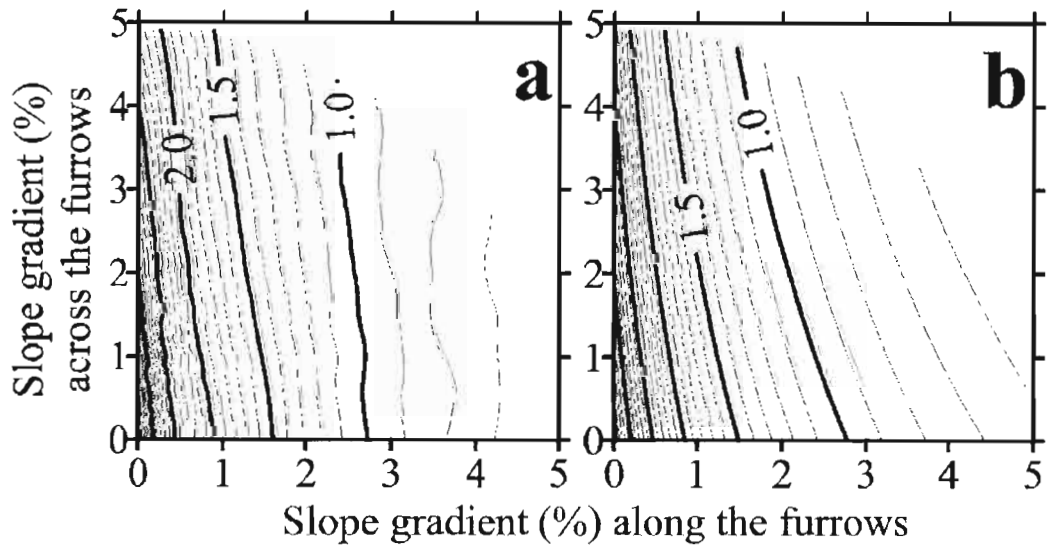


Fig. 9. $\overline{SSC}^{a,b}_{M}$ (mm) related to the slope gradients along and across the furrows: (a) on the microrelief of July 27th; (b) on the modelled tetrahedral container (Eq. (8)).

## 5. Possible application and discussion

When used in hydrological modelling, SSC is most often considered as a constant over large areas. The new characterisation we propose allows us instead to estimate and to map two hydrologic thresholds governing the start of water runoff. The first is the threshold of start of runoff, beyond which water runs along the furrows. The second is the threshold of furrow overflow, beyond which water runs down the slope, crossing the furrows. These two thresholds have been be calculated with the following procedure on the measured plot's watershed:

step 1: microrelief is measured at plot scale ($4 \times 4$ m);
step 2: local slope effect is removed, leading to a zero-slope situation;
step 3: the tetrahedral model is adjusted to this surface with the mirror-BC (tilted in all directions);
step 4: the tetrahedral model is adjusted to this surface with the three-wall-BC (tilted only perpendicularly to the tillage) (steps 1 to 4 have been presented in the previous sections);
step 5: slope angle, slope direction and tillage direction are measured in the watershed with a grid size of 4 m. This gives the maps of slope gradients $L$ and $T$, in the tillage direction and perpendicularly to it, respectively;
step 6: the tetrahedral model calibrated in step 3 is applied to the whole watershed with angles $L$ and $T$ resulting from step 5. This gives the map of the depth of immobile water.
step 7: the tetrahedral model calibrated in step 4 is applied to the whole watershed with angle $T$ resulting from step 5. This gives the map of the depth of water able to flow along the furrows.

Fig. 10 shows the results. Data required to validate this upscaling are not available. Also, it allows us to describe a part of the spatial variability of SSC, the one due to slope and tillage direction. However, the values of the thresholds, as mapped in Fig. 10, must be considered only as an approximation of the reality. It is already known that microrelief interacts with runoff (Govers, 1992; Favis-Mortlock, 1998; Planchon et al., 2000b), so that SSC of a microrelief sampled in a given slope, and numerically tilted as we did, does not follow faithfully the true properties of a microrelief that had been sampled on a different slope.

Further studies, focused on an extensive use of the tetrahedron model, would allow us (a) to define the range of microreliefs for which it can be adjusted and, (b) to study the time and space variability of the depth ratios of the tetrahedral model. Such studies could lead to a better comprehension, and a possible quantification, of the interactions between slope and microrelief.

The scope of the study presented in this paper is similar to that of Darboux (1999), who also is looking at the first stages of runoff. He has shown in particular that runoff starts before SSC is completely filled. He quantified for several types of surfaces the

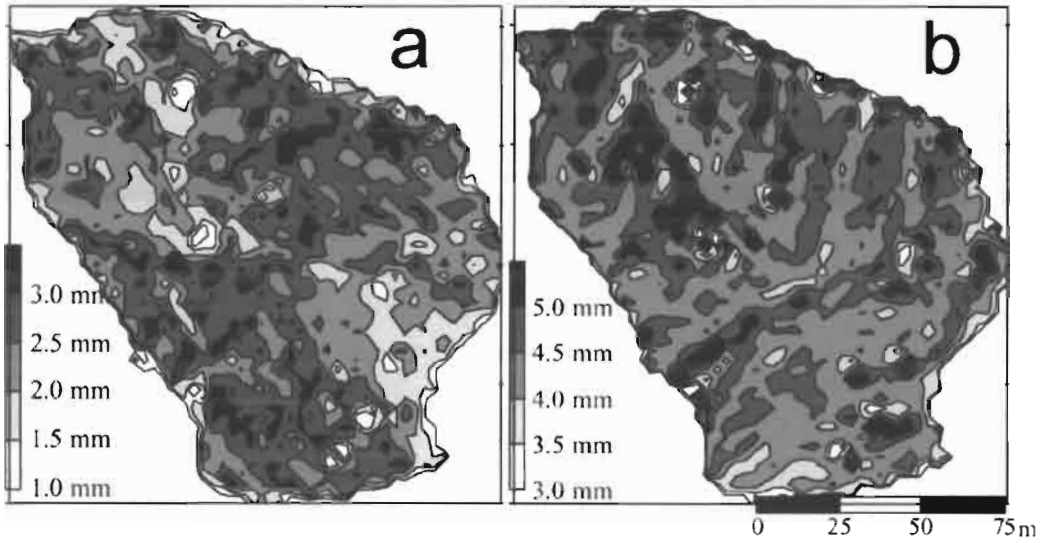


Fig. 10. Use of the tetrahedral model of SSC to map the thresholds of start of runoff along the furrows (a) and of furrow overflow (b).

increase of the runoff coefficient as and when puddles are filled. However, Darboux (1999) only used the three-wall-BC and did not separate out the effect of the slope from that of microrelief. Our approach and Darboux's appear to be complementary and it would be possible and promising to integrate them.

## 6. Conclusion

In this paper, we have shown that the variety of boundary conditions (BC) and of slope extraction leads to varying results on SSC. This problem is exacerbated in tillage-induced microreliefs showing long puddles of which a large number are crossed by the limits of the measured area, making all calculations sensitive to the chosen BC. In that case, the usefulness of classical ways of having SSC values must be totally reappraised.

To overcome this problem, we proposed the calculation of six parameters for SSC instead of its single depth. The six are calculated on the microrelief after the general shape of the plot has been subtracted. The first two are the SSC calculated with the three-wall-BC and the mirror-BC, respectively. Three others are the calibrated depth-ratio parameters describing how the plot empties when tilted. The last parameter represents the part of SSC insensitive to tilt when calculated with the three-wall-BC. The method proposed is above all a geometric description of a given microrelief allowing better characterisation of SSC and its interaction with the slope of the land. It has two major advantages. The first is to use BCs adapted to the tillage-induced microreliefs. The second is to dissociate the effect of microrelief from that of native slope.

The possibility of a proper calibration of our tetrahedral model must be demonstrated on a wider database. A successful follow-through would allow the proposed method to

be used to study the relationship between the microrelief's shape and its native slope, and then lead on to the mapping of the thresholds governing the first stages of runoff.

## References

Allmaras, R.R., Burwell, R.E., Larson, W.E., Holt, R.F., 1966. Total porosity and random roughness of the interrow zone as influenced by tillage. USDA Conserv. Res. Rep. 7, 1–22.

Currence, H.D., Lovely, W.G., 1970. The analysis of soil surface roughness. Trans. ASAE 13, 710–714.

Darboux, F., 1999. Modélisation numérique et expérimentale du ruissellement. Effets de la rugosité sur les distances de transfert. Thèse de Doctorat, Mémoires de géosciences no 93, Université de Rennes, 170 pp.

Favis-Mortlock, D.T., 1998. A self-organising dynamic systems approach to the simulation of rill initiation and development on hillslopes. Comput. Geosci. 24 (4), 353–372.

Gayle, G.A., Skaggs, R.W., 1978. Surface storage on bedded cultivated lands. Trans. ASAE 21, 101–109.

Govers, G., 1992. Relationship between discharge, velocity and flow area for rills eroding loose, non-layered materials. Earth Surf. Processes Landforms 17, 515–528.

Helming, K., Roth, C.H., Wolf, R., Diestel, H., 1993. Characterization of rainfall—microrelief interactions with runoff using parameters derived from Digital Elevation Models (DEMs). Soil Technol. 6, 273–286.

Huang, C.J., Bradford, M., 1990a. Portable laser scanner for measuring soil surface roughness. Soil Sci. Soc. Am. J. 54 (5), 1402–1406.

Huang, C.J., Bradford, M., 1990b. Depressinal storage for Markov–Gaussian surfaces. WRR 26 (9), 2235–2242.

Jenson, S.K., Domingue, J.O., 1988. Extracting topographic structure from digital elevation data for geographic information system analysis. Photogramm. Eng. Remote Sens. 54 (11), 1593–1600.

Jetten, V., de Roo, A., Favis-Mortlock, D., 1999. Evaluation of field-scale and catchment-scale soil erosion models. Catena 37 (3–4), 521–541.

Kamphorst, E.C., 2000. Mesures et méthodes d'estimation de la capacité de stockage d'eau dans le microrelief créé par les opérations de travail du sol. Thèse de doctorat de l'INA PG. 110 pp + Annexes. Institut National Agronomique Paris-Grignon, Paris.

Kamphorst, E.C., Jetten, V., Guérif, J., Pitkänen, J., Iversen, B.V., Douglas, J.T., Paz, A., 2000. Predicting depressional storage from soil surface roughness. Soil Sci. Soc. Am. J. 64, 1749–1758.

Magunda, M.K., Larson, W.E., Linden, D.R., Nater, E.A., 1997. Changes in microrelief and their effects on infiltration and erosion during simulated rainfall. Soil Technol. 10 (1), 57–67.

Mitas, L., Mitasova, H., 1998. Distributed soil erosion simulation for effective erosion prevention. Water Resour. Res. 34 (3), 505–516.

Moore, I.D., Larson, C.L., 1979. Estimating micro-relief surface storage from point data. Trans. ASAE 22, 1073–1077.

Mwendera, E.J., Feyen, J., 1992. Estimation of depression storage and Manning's resistance coefficient from random roughness measurements. Geoderma 52 (3–4), 235–250.

Nearing, M.A., 1998. Why soil erosion models over-predict small soil losses and under-predict large soil losses. Catena 32, 15–22.

Onstad, C.A., 1984. Depressional storage on tilled soil surfaces. Trans. Am. Soc. Agric. Eng. 27, 729–732.

Perez, P., 1994. Genèse du ruissellement sur les sols cultivés du Sud du Saloum Sénégal. Du diagnostic à l'aménagement de la parcelle. Thèse, ENSAM, Montpellier, 250 pp.

Planchon, O., Darboux, F., 2001. A fast, simple and versatile method to fill in the depressions of Digital Elevations Models. In: Auzet, A.V., Poesen, J., Valentin, C. (Eds.), Soil Pattern as a Key Factor of Water and/or Wind Erosion. Catena, pp. 159–176.

Planchon O., Esteves, M., Silvera, N., 1998. Le micro-relief d'un sol sarclé: mesure, modélisation et conséquences sur le ruisselement et l'érosion. AISS XVIeme congrès mondial de Science du sol, 7 pp. + poster, on CD-Rom.

Planchon, O., Esteves, M., Silvera, N., Lapetite, J.M., 2000a. Raindrop erosion of tillage induced microrelief. Possible use of the diffusion equation. Soil Tillage Res. 56 (3–4), 131–144.

Planchon, O., Cadet, P., Lapetite, J.M., Silvera, N., Esteves, M., 2000b. Relationship between raindrop erosion and runoff erosion under simulated rainfall in the Sudano–Sahel. Consequences for the spread of nematodes by runoff. In: Parsons, A.J., Lascelles, B. (Eds.), Rainfall Simulation in Geomorphology. Earth Surface Processes and Landforms, vol. 25(7), pp. 729–741.

Römkens, M.J., Singarayar, M.S., Ganzer, C., 1986. An automated noncontact surface profile meter. Soil Tillage Res. 6, 193–202.

Wilson, B.N., Leaf, R.B., Hansen, B.J., Brown, J.W., Storm, D.E., 1994. Observed surface flow paths from field erosion plots. ASAE paper No. 942049, 24 pp. American Society of Agricultural Engineers (ASAE), St. Joseph, USA.

Zobeck, T.M., Onstad, C.A., 1987. Tillage and rainfall effects on random roughness: a review. Soil Tillage Res. 9, 1–20.